Institutions of the Russian Academy of Sciences
Joint Institute for High Temperatures RAS
Institute of Problems of Chemical Physics RAS
Kabardino-Balkarian State University

# Physics of Extreme States of Matter — 2009

Chernogolovka, 2009

# Physics of Extreme States of Matter — 2009

**Edited by academician Fortov V. E., Karamurzov B. S., Temrokov A. I., Efremov V. P., Khishchenko K. V., Sultanov V. G., Levashov P. R., Kanel G. I., Iosilevski I. L., Milyavskiy V. V., Mintsev V. B., Petrov O. F., Savintsev A. P., Shpatakovskaya G. V.**

This compendium is devoted to investigations in the fields of physics of high energy density and thermophysics of extreme states of matter. Interaction of powerful ion and electron beams with matter, interaction of intense laser, x-ray and microwave radiation with matter, techniques of intense energy fluxes generation, diagnostics of ultrafast processes, physics of shock and detonation waves, different models and results of theoretical calculations of equations of state of matter at high pressure and temperature, low-temperature plasma physics, issues of physics and power engineering, and technology projects are considered. The majority of the works has been presented at the XXIV International Conference on Interaction of Intense Energy Fluxes with Matter (March 1–6, 2009, Elbrus, Kabardino-Balkaria, Russia). The edition is intended for specialists in physical and technical problems of power engineering.

The conference is sponsored by the Russian Academy of Sciences, the Russian Foundation for Basic Research (grant No. 09-02-06056), and the International Science and Technology Center.



**ISBN 978-5-901675-89-2**

# IDEAL MATERIAL STRENGTH, NANOSPALLATION, AND MOLECULAR DYNAMICS SIMULATION BY ADEQUATE EAM INTERATOMIC POTENTIAL

***Zhakhovskii V.V.*[1], *Inogamov N.A.*[*2], *Ashitkov S.I.*[1], *Petrov Yu.V.*[2], *Komarov P.S.*[1], *Nishihara K.*[3]**

[1] *JIHT RAS, Moscow, Russia,* [2] *ITP RAS, Chernogolovka, Russia,* [3] *ILE, Osaka, Japan*

**nailinogamov@googlemail.com*

An irradiation of the condensed matter target by the ultrashort laser pulse (UsLP) of duration $\tau_L$ shorter than the acoustic time $t_s = d_T/c_s$ and shorter than the electron-ion temperature equilibration time $t_{eq}$ (usually $t_{eq} < t_s$) creates the layer with thickness $d_T$ near the target surface with increased temperature and pressure. Subsequent D'Alembert acoustic release of this pressure profile into two acoustic waves penetrating to the left and to the right generates the flow expanding into vacuum and compression wave moving into the bulk from the layer $d_T$ at the irradiated frontal surface. The compression wave appears due to the recoil momentum. The spallation plate runs away from the frontal side if absorbed fluence $F$ is above the threshold for thermomechanical ablation $F_a$ [1–3].

In case of the film the compression wave moves in the direction from the frontal to the rear side surface of the film. If an amplitude of the wave is high enough (this means that $F > F_s$) then its arrival results in the rear side spallation [4, 5]. To differ the frontal and the rear side cases we will call -ablation- the phenomenon of the run away of the plate in the first case. Therefore there are two thresholds: $F_a$ and $F_s$, and $F_s > F_a$.

The work is devoted to experiments and to hydrodynamical and molecular dynamical simulations of such flows. The UsLP is a generator of the compression wave. We use the titanium-sapphire $\tau_L = 40$ fs and chromium-forsterite $\tau_L = 100$ fs lasers. The thickness $d_T$ is very small $\sim 10 - 100$ nm. The smallest thickness corresponds to Si. The thickness $d_T$ defines the thickness of the pressure profile, thickness of the compression wave, and near the thresholds it defines thicknesses of the ablation and spallation plates because (a) the films are thin (the width of the wave is proportional to the way passed by the wave) and (b) the dispersion of the compression wave due to dependence $c_s(\rho)$ is small since the compressions $\Delta\rho/\rho$ are weak at our fluences. This means that the UsLP causes *nanospallation.* The goal of the paper is to achieve extremely high values of the strain rate $\dot{V}/V$ (the last is inversely proportional to $d_T$) and to come as close as possible to the ideal, limiting, or theoretical tensile strength $\sigma_{max}$. The last value is an important material characteristics [6].

The thermomechanical ablation or the rear side spallation begin with nucleation of voids in the stretched melt at the frontal side (ablation) or with generation and amplification of dislocations and after that with appearance of the cracks inside the solid at the rear side (spallation). To describe formation of these voids and cracks we need to take into account the kinetics of associated phase and structural transitions. The most suitable method to calculate these phenomena is the molecular dynamics (MD) simulation because it doesn't contain any phenomenological assumption of phase transition kinetics. The realistic MD simulation requires the adequate description of the interaction between particles forming the target material. For metals we must take into account many-body interatomic interaction due to the conduction electrons. In this work the new many-body embedded-atom method (EAM) potentials for aluminum and gold are proposed. They adequately describe large uniaxial deformations of materials under the action of laser irradiation contrary to other EAM potentials giving a good description of only near-equilibrium states.

The total energy of particles interacting via the EAM potentaial can be written in an ordinary form

$$E_{tot} = \sum_{i<j} V(r_{ij}) + \sum_i F(n_i), \qquad (1)$$

where $V(r_{ij})$ is a pair potential of atoms $i$ and $j$, $F(n_i)$ is the embedding energy of atom $i$ having the "electron" density $n_i$ from its $k-$neighbors: $n_i = \sum_{k\neq i} n(r_{ik})$. Since Daw and Baskes [7] proposed EAM, many forms of its constituent functions were suggested to better describe one or another property of a material. Among the potentials often used recently, the Mishin et al. [8] and the Ercolessi-Adams [9] potentials should be mentioned (both use the cubic spline fit of EAM functions). The ordinary parameters of potentials [8, 9] are chosen to represent data on condensed matter near the normal condition for the equilibrium state. In the case of ablation of a metal target under the action of UsLP we are interested in description of a target matter subjected to considerable deformations mainly in the direction of a laser pulse and as was said the interaction potential should take into account such large deformations. We have constructed the many-body potential for aluminum and gold in the frame of embedded atom model which adequately describes these deformations. For Al the EAM potential functions are taken in the analytical form:

$$\begin{aligned} x &= a_1 r^2, \quad x_c = a_1 r_c^2, \\ V(r) &= (1/x - a_2)(x - x_c)^{10}[(x - x_c)^6 + a_3 x^6] \quad (2) \\ F(n) &= b_1 n(b_2 + (b_3 + n)^2)/(1 + b_4 n) \quad (3) \\ n(r) &= c_1(r^2 - r_c^2)^2/[1 + (c_2 r^2)^3] \quad (4) \end{aligned}$$

with $r_c = 0.6875$ nm being the cutoff radius. Parameters $a, b, c$ were chosen to minimize difference between the values of cold pressure tensor of strongly deformed metal evaluated by the use of our EAM potential and by ABINIT code [10] in addition to the agreement with known experimental parameters of Al at low temperatures. Detailed comparisons of cold pressure components obtained by our new Al EAM potential and Mishin et al. potential will be published in [11].

Similar form of EAM potential was proposed for gold with a small change of the pair interaction potential.

**Table 1.** EAM potentials Eqs.(2-5) for aluminum and gold. Energy in kJ/mole units.

| N | $a_N$ in $V(r)$ for Al | $a_N$ in $V(r)$ for Au |
|---|---|---|
| 1 | 2.9275228176598036 | 2.7471581015136728 |
| 2 | 5.1028014804162156 | 5.3593750000000000 |
| 3 | 111.37742236893590 | 3.2500000000000000 |
| N | $b_N$ in $F(n)$ for Al | $b_N$ in $F(n)$ for Au |
| 1 | 8.1106000931637006 | 8.2311259601633768 |
| 2 | -334.57493744623503 | -382.38931538388255 |
| 3 | 14.868297626731845 | 16.250071667347235 |
| 4 | 1.6080953931773090 | 1.4586663896542300 |
| N | $c_N$ in $n(r)$ for Al | $c_N$ in $n(r)$ for Au |
| 1 | 0.58002942432410864 | 3.0697898737897571 |
| 2 | 8.2981185422063639 | 20.750105835621902 |

It was chosen in the form

$$V(r) = (1/x - a_2)(x - x_c)^{10}((x - x_c)^{18} + a_3) \quad (5)$$

Our new Au EAM potential shows a good agreement with cold pressure evaluated by ABINIT for large stretching (description of hydrodynamic rarefactions) as well as for large compression ratio (description of strong shocks).

New EAM potentials can be tested by the calculation of activation energy of diffusion. Vacancy migration energy $E_{vm}$ has different values for fixed positions of surrounding atoms ($E_{vmu}$) and for crystal lattice relaxed to its energy minimum ($E_{vm}$). For our Al EAM potential $E_{vmu}$ = 90.39 kJ/mole while $E_{vm}$= 56.01 kJ/mole. Together with the vacancy formation energy $E_{vfu}$=72.92 kJ/mole for the case of unrelaxed lattice and $E_{vf}$=72.01 kJ/mole when allowing for relaxation it gives the activation energy of diffusion $E_D = E_{vf} + E_{vm}$=128.02 kJ/mole. This value is in a good agreement with the experimental one 128.3 kJ/mole [12].

The formation, propagation, and beginning of breaking of the compression wave is presented in Fig. 1. The breaking results in formation of a shock marked by the arrow $S_f$. After its formation the pressure jump in the shock front increases as the shock moves faster relative to the precursor forward to the shock and moves slower relative to the remnant of the smooth profile of the compression wave. The traces of the smooth compression wave profile almost disappear after passing the distance $L$ = 700 nm. This distance is the thickness of the film used in the simulation. The value $L$ influences the time dependences shown in Fig. 2 and 3, see discussion below. $L$ = 300 nm in the experiment presented in Fig. 4. The strength shown in Fig. 5 also depend on the profile of the compression wave impacting the rear side.

In our range of fluences for Al the heat penetration $d_T$ varies weakly with absorbed fluence $F$. Therefore $F$ and $T_s$ defined in the capture to the Fig. 1 are approximately proportional ($T_s \propto F$) and the normalized fluence and temperature are approximately equal $F/F_a \approx T_s/(T_s)_a$, where $(T_s)_a$ is the maximal electron-ion equilibration temperature at the ablation threshold. The proportionality $T_s \propto F$ is valid because at our fluences at the electron-ion thermal equilibration stage the electron heat capacity is small and the ion heat capacity is approximately constant (the Dulong-Petit law).

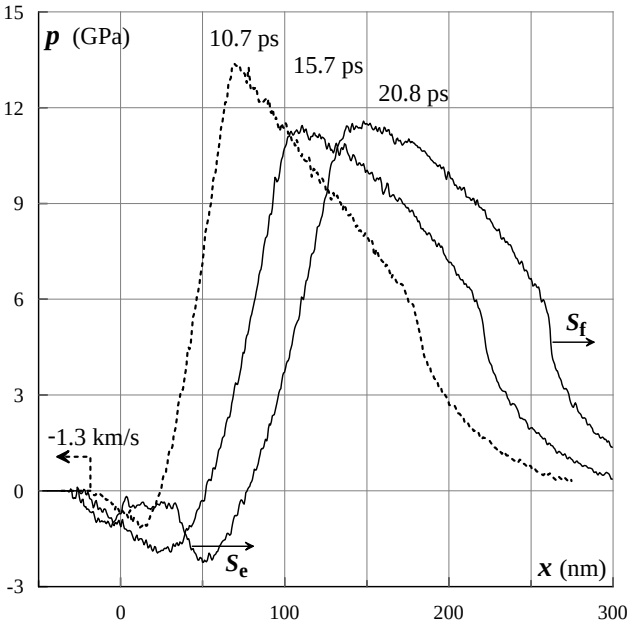


**Figure 1.** Evolution of the compression wave and beginning of its breaking. Al, $F/F_a = 2.2$, $T_s = 5$ kK, here $F$ is absorbed fluence, $T_s$ is the maximum temperature at the instant of the $T_e$ and $T_i$ equilibration after two-temperature relaxation [1]. The compression wave is created by the pump UsLP with maximum intensity achieved at the instant $t = 0$ (the origin of the time axis).

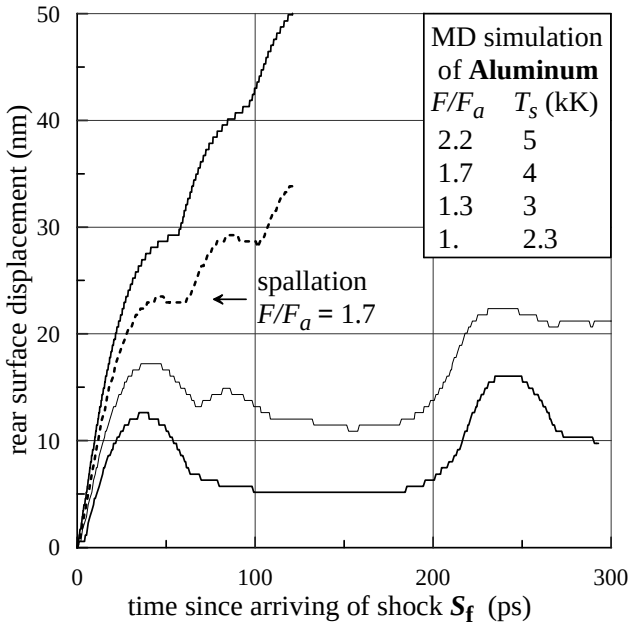


**Figure 2.** The trajectory of the rear side surface of the film resulting from an action of the compression wave shown in previous Figure. This wave and therefore the rear side displacement appear owing to the D'Alembert sonic decomposition and the recoil momentum created at the frontal side by the pump UsLP.

Arrival of the compression wave (Fig. 1) at the rear side causes displacement of the rear side illustrated in

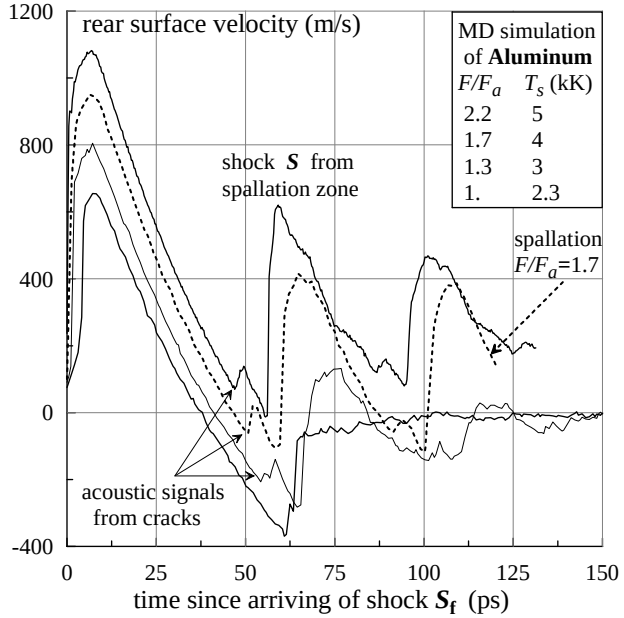


**Figure 3.** Velocity of the rear side. It is the time derivative of the trajectory shown in previous Figure.

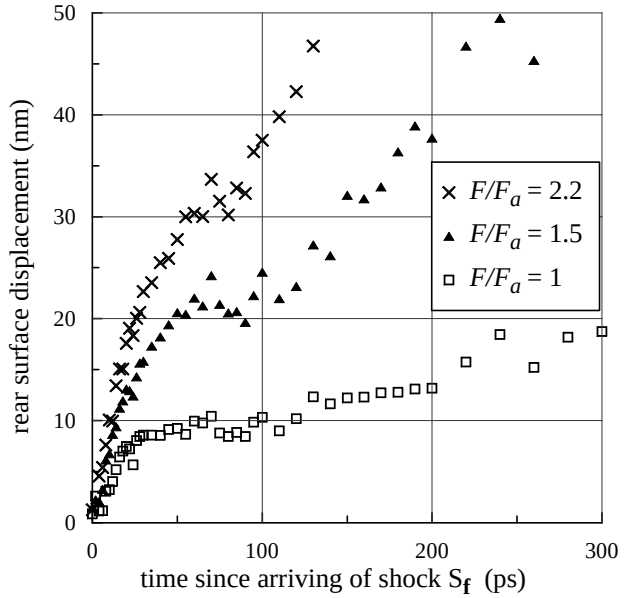


**Figure 4.** Experimental displacement of rear surface of Al film 300 nm thick. In this Figure the $F$ and $F_a$ in the normalized ratio $F/F_a$ correspond to the incident fluence $F_{inc}$ and to ablation threshold $(F_{inc})_{abl}$ taken for $F_{inc}$. In other cases $F$ means the absorbed fluence as it is stated above. The important nonlinear absorption function $F(F_{inc})$ for the Al target and the pump UsLP used in our experimental setup with the chromium-forsterite laser ($\tau_L = 100$ fs, $\lambda_{pump} = 1240$ nm, the angle of incidence is $45^o$, and p-polarization) is presented in [4].

Figs. 2 and 4. Corresponding velocities are shown in Fig. 3. There is the velocity jump induced by arriving of the shock $S_f$ in the last Figure. The value of the jump depends on the amplitude of the compression wave growing with the absorbed fluence $F$. After the jump up the velocity in Fig. 3 decreases down until arriving of the shock S from the frontal ablation zone. The velocity decreases $\Delta u \approx 1.1$ km/s, defined as a

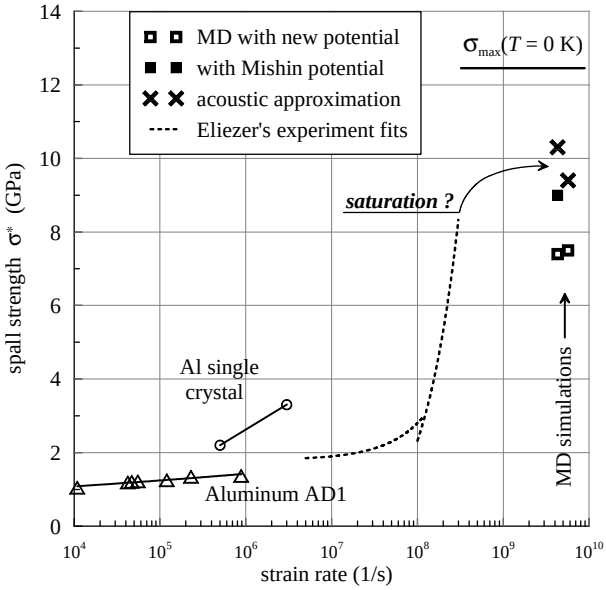


**Figure 5.** Hardening of Al relative to the stretching rate $\dot{V}/V$ [6]. The Al single crystal and AD1 dots correspond to the explosive experiments. They are taken from [13]. The two dotted curves present laser experiments with rather long pulses [14]. The empty squares give the local values of $\sigma$ and $\dot{V}/V$ at the instant just before beginning of the subsequent fragmentation for $T_s = 4$ and 12 kK or $F/F_a = 1.7$ and 5.2. This is the case of the UsLP creating extremely high $\dot{V}/V$. The corresponding acoustic approximations calculated from the velocity decrease $\Delta u$ (see Fig. 3) in the linear expression (6) are indicated by the two diagonal crosses. The filled square represents the local values for the potential [8] with $T_s = 6$ kK. The limiting strength $\sigma_{max}$ marked with the horizontal straight corresponds to the uniform 3D expansion of Al crystal in the new EAM potential. In the case of the uniaxial stretching the strength $\sigma_{max}$ depends on the direction of stretching.

difference between the maximum (just after arrival of the shock $S_f$) and minimum (just before the arrival of the shock S) velocities, can be used in linear acoustic approximation [13] to obtain the spall strength of material from expression

$$\sigma^* = \rho_0 c_l \Delta u/2, \qquad (6)$$

where $\rho_0$ is initial density and $c_l = 6.9$km/s is sound speed along $\langle 110 \rangle$ directions of the ideal fcc Al EAM crystal. The velocity decrease $\Delta u$ takes place as a result of resistance of condensed phase to stretching. Expression (6) gives the spall strength of 10.3 GPa (the upper diagonal cross in Fig. 5), which is significantly higher than simulated one 7.4 GPa (the empty square in Fig. 5). This is the result of significant decrease of sound speed with stretching (because the larger stress $\sigma$ is created by the larger deformation) in our case with amplitude of deformation larger than in any other case presented so far.

In the pump-probe experiments with microinterferometric fringes [2] the displacements shown in Fig. 4 are measured. These technique is equivalent to the measurements done by the VISAR or ORVIS, see, e.g., [14], at much larger space-time scales.

The experimental and simulated displacements shown in Fig. 4 and 2 are similar in their integral char-

acteristics (amplitude, duration). Though the experimental and calculated conditions differ. The freestanding Al film are considered in the simulation. It has two boundaries with vacuum and its thickness $L$ is 700 nm. The experimental Al film is thinner ($L = 300$ nm). It is deposited at the thick glass plate (thickness of the plate is 150 um). The pump UsLP heats the film from the glass plate side penetrating through glass. It initiates compression wave propagating from the glass/Al boundary. This boundary is the frontal side in the experiment. As was said, the arrival of this wave at the rear side causes the displacements illustrated in Fig. 4. Hence there are two differences between the simulation and the experiment: (i) the film is thinner (300 nm instead of 700 nm). Therefore the shock $S_f$ in Fig. 1 only begins to form when it arrives at the experimental rear side. This instant approximately corresponds to the last profile presented in Fig. 1. (ii) In the simulation the frontal side is free (the vacuum boundary), while in the experiment it is closed by the glass plate. The glass does not change the forward part of the profile from beginning of the wave up to the maximum of pressure. But the subsequent part of the profile is formed by the D'Alembert wave reflected from the frontal boundary. Therefore this part of the pressure profile is different from shown in Fig. 1. The initial velocity rise in Fig. 3 does not depend on the mechanical frontal boundary condition if the absorbed energies are equal. But the subsequent velocity dependence and the rear side trajectory are functions of the second part of the pressure profile. In spite of these differences the dependences in Figs. 2 and 4 are similar because the amplitudes and durations are similar.

The calculated values for the material strength are presented in Fig. 5. Our simulations and experiments correspond to the record values of $\sigma$ and $\dot{V}/V$. The experimentally measured values calculated from data shown in Fig. 4 will be added to Fig. 5 in near future. To do this we have to estimate better the velocity decrease $\Delta u$ (it appears due to material resistance) from the measured displacements. In MD simulation the crystal without defects is used as initial state. The MD points in Fig. 5 may be or continuation of the two points for Al crystal, or the saturation level for the polycrystalline case given by the dotted curve. The MD results shown in Fig. 5 depend on the EAM potential. This opens the way to the experimental check of the EAM parameters.

The work is supported by the RFBR grant No. 07-02-00764.

1. Anisimov S. I., Inogamov N. A., Petrov Yu. V. *et al.* // Appl. Phys. A 2008. V. 92. P. 939.
2. Inogamov N., Zhakhovskii V., Ashitkov S. I. *et al.* // JETP 2008. V. 107. P. 1.
3. Povarnitsyn M. E., Itina T. E., Sentis M. *et al.* // Phys. Rev. B 2007. V. 75. P. 235414.
4. Anisimov S. I., Inogamov N. A., Petrov Yu. V. *et al.* // Appl. Phys. A 2008. V. 92. P. 797.
5. Ivanov D. S. and Zhigilei L. V. // Phys. Rev. B 2003. V. 68. P. 064114.
6. Fortov V. E. Powerful Shock Waves and Extreme States of Matter. The Scientific Lecture given on the Occasion of the Investiture of the Large International Gold Medal named after A. Einstein for Physics. M.: Bukos, 2005. [In Russian].
7. Daw M. S. and Baskes M. I. // Phys. Rev. B 1984. V. 29. P. 6443.
8. Mishin Y., Farkas D., Mehl M. J. *et al.* // Phys. Rev. B 1999. V. 59. P. 3393.
9. Liu X.-Y., Ercolessi F., Adams J. // Modelling Simul. Mater. Sci. Eng. 2004. V. 12. P. 665.
10. The ABINIT code is a common project of the Universite' Catholique de Louvain, Corning Incorporated, and other contributors (http://www.abinit.org).
11. Zhakhovskii V., Inogamov N., Petrov Yu. *et al.* 6-International Conference on Photo-Excited Processes and Applications 9-12 Sep 2008, Sapporo, Japan, accepted for publication in Applied Surface Science (2009).
12. Dais S., Messer R., Seeger A. // Mat. Sci. Forum 1987. V. 15-18. P. 419.
13. Kanel G. I., Razorenov S. V., and Fortov V. E. Shock-Wave Phenomena and the Properties of Condensed Matter. (Eds) L. Davidson, Y. Horie. Springer, 2004.
14. Eliezer S., Moshe E., and Eliezer D. // Laser and Particle Beams 2002. V. 20. P. 87.

## EXPERIMENTAL AND THEORETICAL INVESTIGATION OF OPTICAL AND TRANSPORT PROPERTIES OF ALUMINUM PLASMA UNDER INTENSE FEMTOSECOND LASER PULSES

***Komarov P.S., Ashitkov S.I., Ovchinnikov A.V., Sitnikov D.S., Veysman M.E., Levashov P.R., Povarnitsyn M.E., Agranat M.B., Andreev N.E., Khishchenko K.V.*, Fortov V.E.***

*JIHT RAS, Moscow, Russia*

**konst@ihed.ras.ru*

**Introduction.** The optical and transport properties of strongly coupled plasma formed on the surface of an aluminum target irradiated by femtosecond laser pulses with the intensity $I \lesssim 10^{15}$ W/cm$^2$ have been studied both experimentally and theoretically. Such laser pulses produce a thin layer of the solid-density plasma with an electron temperature up to $T_e \simeq 60$ eV. We studied the initial stage ($t \leqslant 1$ ps) of the heating and expansion of the plasma under the conditions of the undeveloped hydrodynamic motion of ions. The present work continues our previous experimental and theoretical investigations of aluminum [1] and silver [2] plasmas under the influence of femtosecond laser pulses on solid targets in the range of intensities up to $I \sim 10^{14}$ W/cm$^2$.

**Experiment.** A source of radiation is a terawatt chromium-doped forsterite laser system that generates femtosecond pulses at the wavelength of 1.24 $\mu$m [3].